[Article ID] 1003- 6326(2001)01- 0084- 06

Microstructures of rapidly solidified Al-In immiscible alloy①

LIU Yuan(刘 源), GUO Jing-jie(郭景杰), SU Yan-qing(苏彦庆),
DING Hong-sheng(丁宏生), JIA Jun(贾 均)
(School of Materials Science and Engineering,
Harbin Institute of Technology, Harbin 150001, P. R. China)

[Abstract] The microstructural evolution and growth mechanism of the melt spun Al-In monotectic alloy were studied. During the rapid solidification of Al-17.5% In, a cellular structure→equiaxed structure transition occurs through the ribbon thickness. The as-solidified microstructures are characterized by a homogeneous distribution of nanometer sized indium particles embedded within the matrix. However, with increasing distance from the chilled surface, the average particle size increases. In the underside of the ribbon, some particle arrays are perpendicular to the growth front. Next, all of the indium particles distribute randomly within the matrix. In the upside of the ribbon, some bigger indium particles distribute along the equiaxed grain boundaries. The diameter distributions of indium particles within Al matrix are bimodal. Compared with the massive partitionless solidification, the liquid separation process is the prevailing process during the non-equilibrium solidification. The cooling rate, the interface energies ($\gamma_{S1/L1}$, $\gamma_{S1/L2}$ and $\gamma_{L1/L2}$) and the growth mechanism all have effects on the microstructure.

[Key words] Al-In immiscible alloy; rapid solidification; microstructure
[CLC number] TG249.7 [Document code] A

1 INTRODUCTION

There are many binary immiscible systems with a miscibility gap which have been identified as desirable for many applications, such as engineering and electronic materials, high temperature superconductors, and self-lubrication bearings[1~3]. However, the fabrication of such systems by conventional melting and casting techniques poses serious problems, which arise from a negligible mutual solid solubility and a large miscibility gap in the liquid state. This results in severe gravity segregation in casting due to the large density difference between two liquid phases ($L1$ and $L2$). It is, therefore, difficult to disperse the second phase uniformly in a host matrix.

Before 1970, people rarely considered the practical applications of immiscible alloys because of the limited understanding of their liquid-liquid phase separation mechanism. By now, people have had a relatively clear understanding of their phase separating process as well as those factors influencing the separating process[4~6]. Recently, with the development of the preparation techniques, researchers are interested in preparing homogeneous immiscible alloys. It is expected that microgravity conditions would result in a homogeneous dispersion of the second phase during monotectic reaction, but this has proven to be not the case[7]. In general, rapid solidification is reported to promote a random dispersion of the second phase[8]. Unfortunately, almost all the studies related to rapid solidification to date deal with either eutectics or peritectics and a limited study is known to immiscible alloys. The authors prepared Al-In immiscible alloy by melt spinning and studied its morphology evolution during rapid solidification in the present paper. It is of vital importance for controlling the microstructures and developing their applications.

2 EXPERIMENTAL PROCEDURE

Al-17.5% In alloy charges approximately 5 g made up of 99.99% pure aluminum and indium were induction melted in quartz crucible under a dynamic argon atmosphere, held for 300 s at 1 000 ℃ and ejected with an argon overpressure of 80 kPa through a 12 mm diameter orifice onto the outer surface of a polished copper wheel rotating with a tangential speed in the range of 10~ 40 m/s. The resulting melt spun ribbons are typically 40~ 200 μm in thickness, and 7 ~ 9 mm in width. Specimens cut from the melt spun ribbon were ion thinned and jet electropolished in a mixture of 25% nitric acid and 75% methanol at - 40 ℃, respectively, to fit for the microstructural examination in a Philips EM420 TEM operating at 120 kV and EPMA examination.

3 EXPERIMENTAL RESULTS

Figs. 1(a) ~ (d) show typical bright field TEM images taken at the center position of Al-17.5% In ribbons melt spun at the wheel speeds of 13 m/s, 18 m/s, 27 m/s and 36 m/s. It can be seen that fine

① [Foundation item] Project (9- 04) supported by Emersion Foundation of USA
[Received date] 2000- 03- 09; [Accepted date] 2000- 08- 28

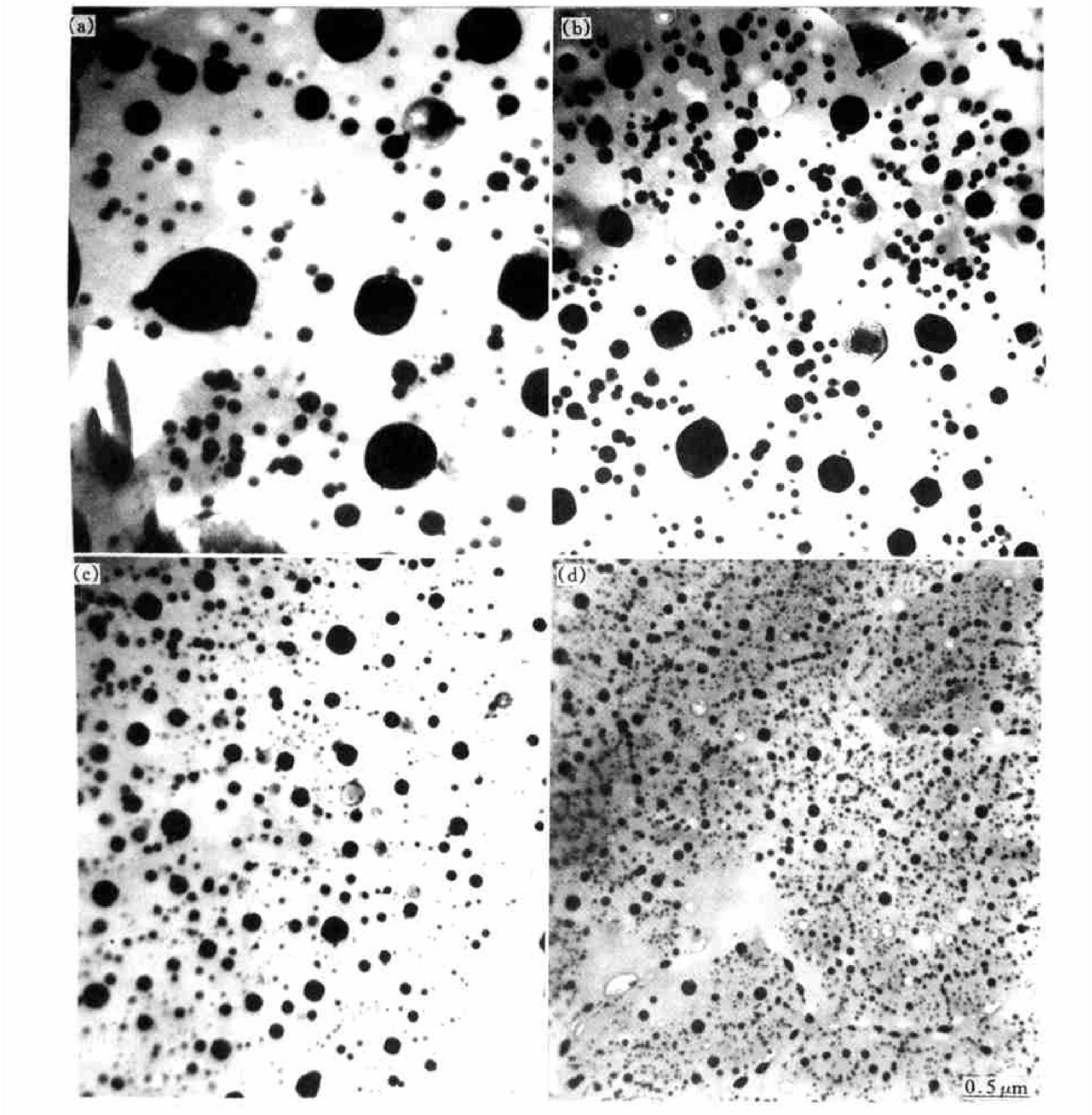

Fig. 1 Typical bright field TEM images taken at center position of Al-18% In ribbons melt spun at various wheel speeds
(a) —v_s= 13 m/s; (b) —v_s= 18 m/s; (c) —v_s= 27 m/s; (d) —v_s= 36 m/s

nanometer sized indium particles distribute homogeneously within the matrix, but the average size of indium particles as well as the size difference between the smallest and the biggest particles decreases with increasing wheel speed. The indium particles are faceted, as shown in these figures, corresponding to truncated octahedral particle shapes by $\{111\}_{Al}$ facet and exhibited orientation relationship with the surrounding aluminum matrix, described as $\{111\}_{Al} \parallel \{111\}_{In}$ and $\langle 110\rangle_{Al} \parallel \langle 110\rangle_{In}$ which is resulted from the anisotropic surface-energy[9]. It is also found that there exist some clear cellular boundaries in Figs. 1(c) and (d). Additionally, particle-free zones of 0.2~0.4 μm in thickness are often found adjacent to the aluminium cellular boundaries, sometimes being accompanied with larger indium particles surrounded by a particle-free zone. Due to a higher cellular spacing as well as the zone of vision not located at the boundaries, this kind of structure can not be seen in Figs. 1 (a) and (b). This kind of structure is also seen in

Fig. 2—the image near the chilled surface of Al-17.5% In ribbon melt spun at the wheel speed of 18 m/s. Figs. 3(a) ~ (d) show the diameter distributions of indium particles, from which it can be found: 1) the diameter distributions are bimodal for all the wheel speeds; 2) the bimodal distribution becomes obscure with increasing wheel speed.

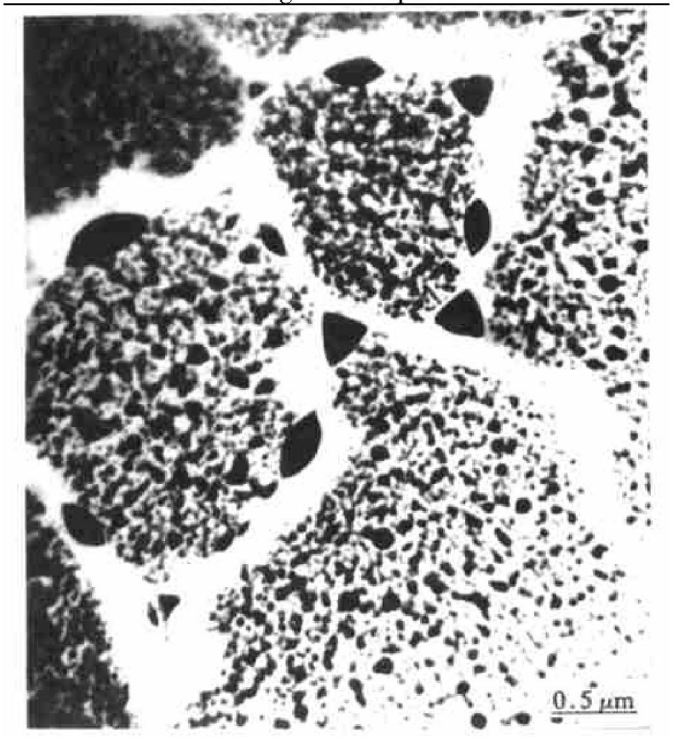

Fig. 2 Typical bright field TEM image taken near chilled surface of Al-17.5% In ribbon melt spun at wheel speed of 18 m/s
(There exist cellular structure and particle-free zones)

Figs. 4(a) ~ (c) show the typical back-scatted electron images at different positions of the cross-section of Al-17.5% In melt spun at the wheel speed of 13 m/s. Fig. 4(d) shows the surface map of indium corresponding to Fig. 4(c). Figs. 5(a) and (b) show the back-scattered electron images on the cross-section of Al-17.5% In melt spun at the wheel speed of 27 m/s. On the whole, indium particles distribute homogeneously within the Al matrix. However, the particle size and its morphology are different through the thickness of Al-In ribbons. With increasing distance from the chilled surface, the average particle size increases. Additionally, in the underside of the cross section, as shown in Fig. 4(a) and Fig. 5(a), some particles array perpendicularly to the growth front. With increasing distance from the chilled surface, the indium particles randomly distribute within the matrix (Figs. 4(b) and (c) and Fig. 5(b)). In the upside of the cross section, if the wheel speed is lower and the ribbon thickness is higher, as shown in Fig. 4(c), some bigger indium particles are found to distribute along the equiaxed grain boundaries. But when the wheel speed is higher and the ribbon is thinner, in the same field, as shown in Fig. 5(b), this kind of phenomenon cannot be found.

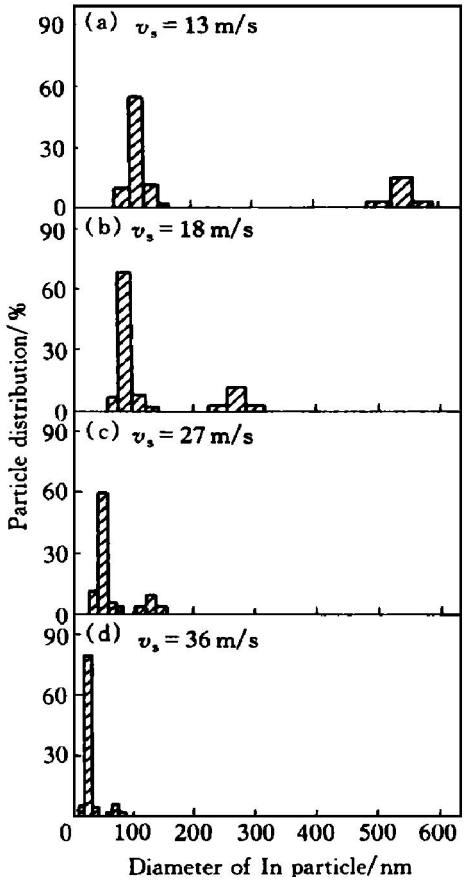

Fig. 3 Diameter distribution of indium particles in melt spun Al-17.5% In under various wheel speeds

4 DISCUSSION

4.1 Pathway for microstructure evolution under non-equilibrium solidification condition

A metastable phase diagram can reveal an alternative possibility of microstructure selection under extreme non-equilibrium solidification conditions such as rapid solidification. A schematic of such a metastable diagram is shown in Fig. 6. The figure also includes equal free energy line (T_0) of solid and liquid. A liquid-solid transformation without any composition change (also called as massive solidification) by a non-equilibrium solute trapping process is thermodynamically feasible in the region below equal free energy curve T_0 in spite of strong clustering tendency due to positive heat of mixing. In Fig. 6 the domain with hatching is a regime where exist two feasible processes on thermodynamics: the first is the liquid separation and the following trapping of second-phase liquid droplets in the solid matrix; the second is the massive partitionless solidification and the subsequent decomposition process in the solid state. In such case the relative kinetics of the two processes would determine the pathway of the microstructural evolution. An idea of the prevailing kinetics in this region can be obtained by calculation of the critical nucleation tem-

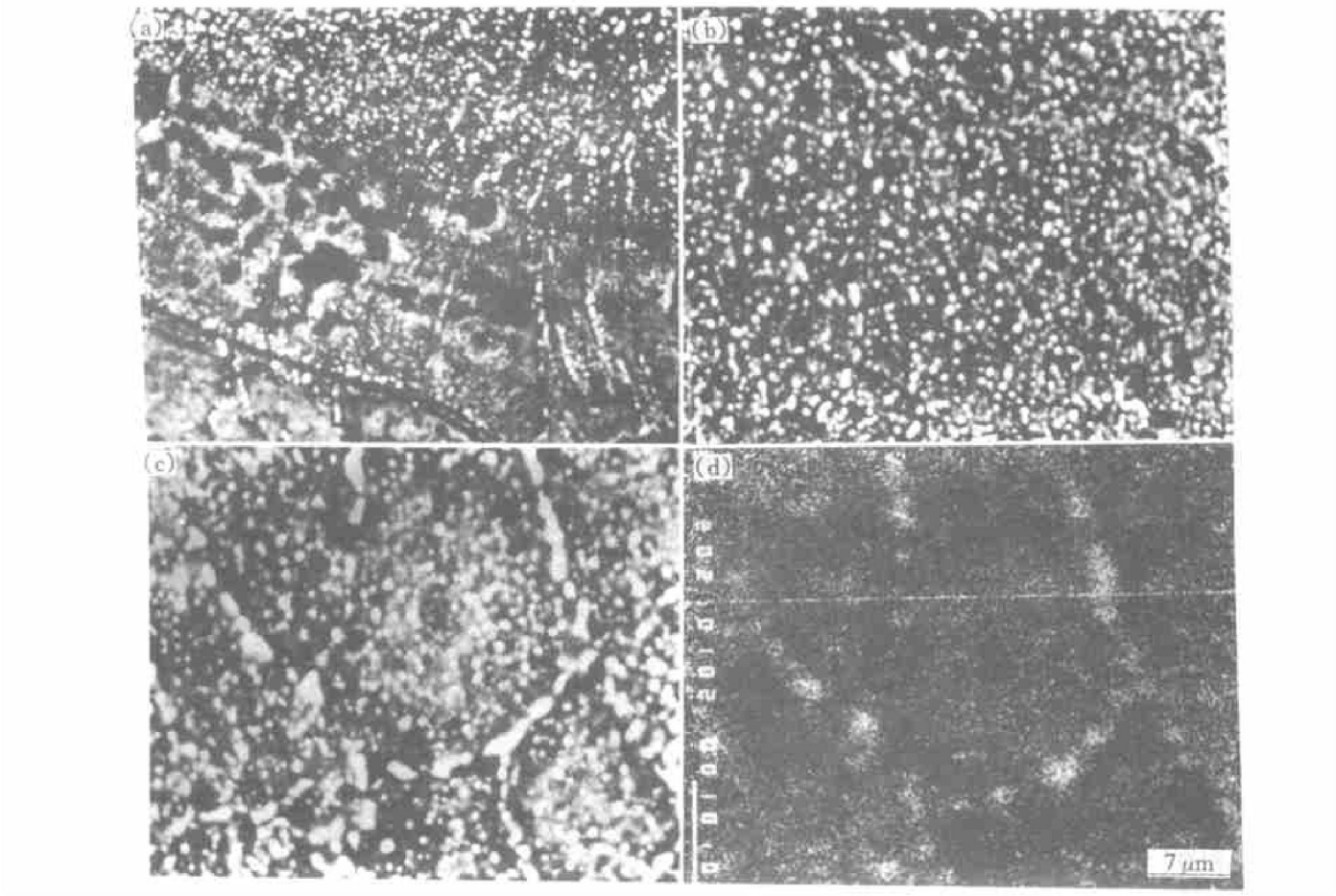

Fig. 4 Typical back-scattered electron images taken on various positions of cross-section of Al-17.5% In ribbons melt spun at wheel speed of 13 m/s
(a) —Underside; (b) —Central; (c) —Upside; (d) —Surface distribution of indium corresponding to (c)

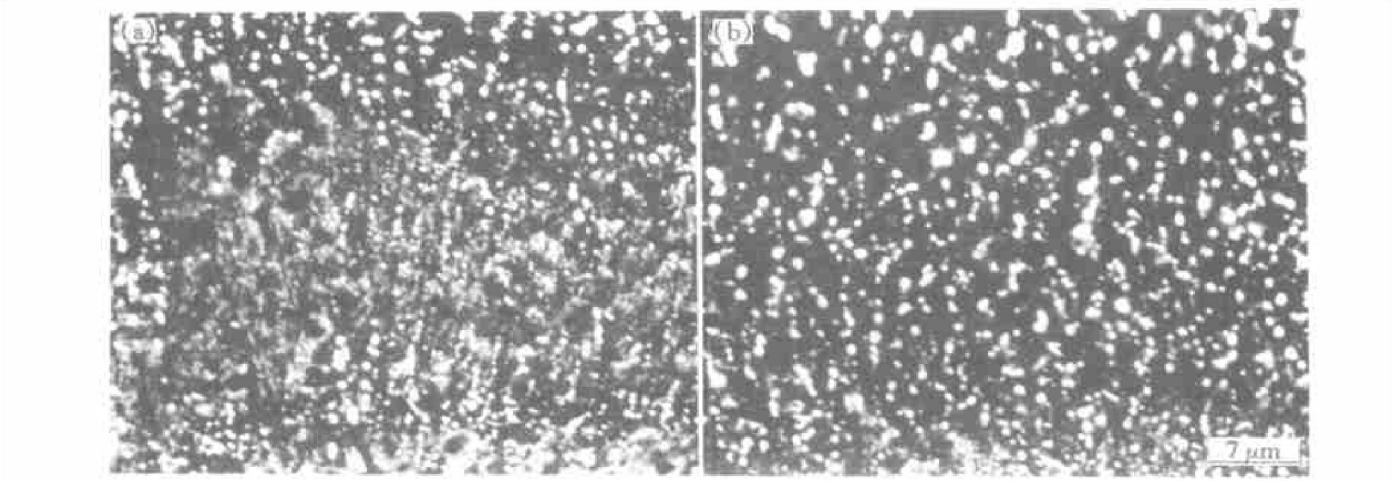

Fig. 5 Typical back-scattered electron images taken on various positions of cross-section of Al-17.5% In ribbons melt spun at wheel speed of 27 m/s
(a) —Underside; (b) —Upside

perature of the second phase (T_N) as a function of composition in this regime[10]. If $T_N > T_0$, liquid separation cannot be prevented and the microstructure will always evolve by trapping this second liquid ($L2$). If $T_N < T_0$, the massive transformation of solid and its subsequent decomposition represent a highly probable pathway.

It is well known that the diameter distribution of second phase particles should be bimodal if the solidification of an immiscible system undergoes the liquid separation process. The bigger particles are formed during cooling through the region of liquid immiscibility while the smaller particles are formed during monotectic solidification of the matrix[11]. The diameter distribution of indium particles in Al matrix, as shown in Fig. 3, is just bimodal, so it can be conclud-

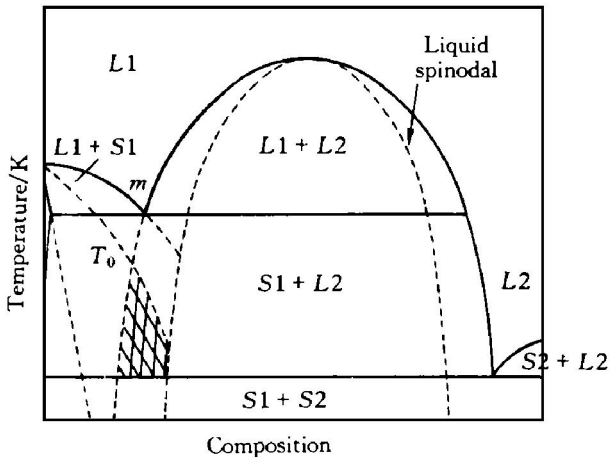

Fig. 6 Schematic non-equilibrium diagram of immiscible system

ed that the liquid separation process is the prevailing process during the non-equilibrium solidification of Al-17.5% In immiscible alloy. The calculated results of T_N and T_0 shown in Fig. 7 also testify this conclusion. With the increase of the wheel speed, as shown in Figs. 1(a) ~ (d), the indium rich liquid ($L2$) thus formed will become smaller due to limited time available for its growth, so the bimodal distribution may become obscure, just as shown in Fig. 3(d). On the other hand, this process will enrich the remaining liquid with indium and will effectively increase T_0 temperature and decrease T_N temperature, consequently, the remaining liquid may undergo a massive solidification and subsequent solid decomposition process. Because the solid decomposition is a diffusion process in solid, so its products are very fine. In such a case, the second phase particles will be very fine, just as shown in Fig. 2(d).

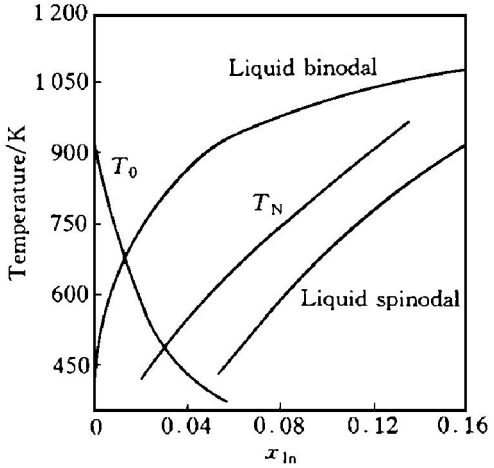

Fig. 7 Calculated T_0 and T_N of Al-In immiscible alloy

4.2 Growth mechanism and particle morphology

With the help of the above microstructural observation, it is possible to understand the growth mechanism of Al-In immiscible alloy. At extreme growth rates when the interface growth rate is higher than the rate of diffusion of the solute, the latter will be trapped in the growing matrix and there does not exist a solute boundary layer in front of the interface. In such a case, the shape of the interface will be plane due to the single direction of the heat transfer normal to the chilled surface. However, as the growth rate decreases, solute will start to diffuse at the interface. Correspondingly, the plane front will break down due to a solute boundary layer and a cell structure will be formed. In this paper, in the underside of the Al-17.5% In ribbons melt spun at selected wheel speeds, the growth rate is not so great that a cell structure is formed. But when the wheel speed is lower and the ribbon thickness is higher, because the cooling rate decreases, especially because the effect of the radiation from the free surface as well as conduction causes multi-directional heat transfer, in the upside of the ribbon, the matrix phase appears as equiaxed grains. In other words, a cellular structure → equiaxed structure transition occurs through the ribbon thickness

It is well recognized that the nature of the two phases ($S1$ and $L2$) as solidified microstructure primarily depends on the three interface energies involved in the monotectic growth, namely $\gamma_{S1/L1}$, $\gamma_{S1/L2}$ and $\gamma_{L1/L2}$[12]. Fig. 8 shows schematic temperature variations of the $\gamma_{S1/L1}$, $\gamma_{S1/L2}$ and $\gamma_{L1/L2}$. Below the critical wetting temperature T_W, because $\gamma_{S1/L2} < \gamma_{S1/L1} + \gamma_{L1/L2}$, $L2$ phase can wet $S1$ phase, as a result, a three phase equilibrium at the growth interface is possible. In such a case, the low growth rate can lead to a cooperative growth between $S1$ and $L2$. During the rapid solidification process, as shown in Fig. 9(a), the growing liquid phase often becomes unstable behind the growth front leading to an arrayed particle morphology. On the other hand, an increasing growth rate may lead to a breakdown of the diffusion couple necessary for sustaining cooperative growth at some position. This leads to a morphology shown in Fig. 9(b). When the growth rate is very high, a complete breakdown of the diffusion

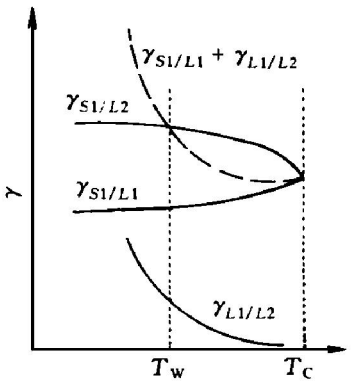

Fig. 8 Schematic variations of $S1/L1$, $S1/L2$ and $L1/L2$ interfacial energies as function of temperature

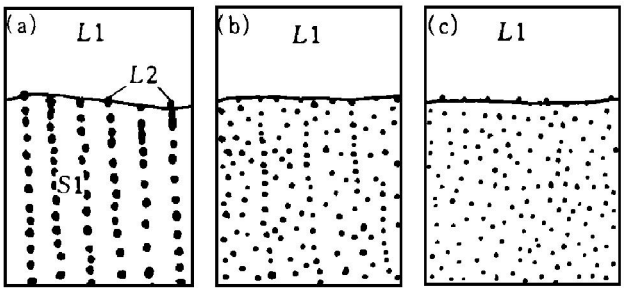

Fig. 9 Schematic diagrams of particle morphologies as function of growth rate of $S1$ (v_{S1})
(a) —Low v_{S1}; (b) —Medium v_{S1}; (c) —High v_{S1}

couple leads to a random particulate morphology as Fig. 9(c).

According to the critical wetting theory, the critical wetting temperature T_W of the Al-In alloy is higher than its monotectic temperature T_m[13]. For Al-17.5% In immiscible alloy, the nucleation temperature of $L2$ is below the T_m. Therefore, a three phase junction can form at the growth front. In the underside of the melt spun ribbons, as shown in Fig. 4(a) and Fig. 5(a), a higher growth rate leads to a morphology analogous to Fig. 9(b). In the central and upside of the ribbon's cross section, although the lower growth rate will lead to an arrayed particle perpendicular to the growth front, the multi-directional growth of $S1$ and the flow of $L2$ droplets in the flowing fluid lead to a macroscopical random particulate morphology as Figs. 4(b) and (c) and Fig. 5(b). In addition, in the upside of the melt spun ribbon, the lower growth rate of the matrix will push a large amount of solute into the grain boundaries, finally, as shown in Fig. 4(c), lead to the distribution of large sized indium particles along the equiaxed grain boundaries.

The existence of particle-free zones is a common phenomenon for many immiscible systems. Among the several mechanisms considered to explain the formation of particle-free zones[12], the authors think that the droplets migration in the liquid is reasonable. In the later stage of solidification of each grain, many $L2$ droplets may be pushed ahead of the $S1$ into the grain boundaries. The grain boundary is so strait that the collision among many droplets leads to the form of particle-free zones, being accompanied with larger indium particles in it.

[REFERENCES]

[1] Inoue A and Yano N. Microstructure and superconducting properties of melt-quenched insoluble Al-Pb and Al-Pb-Bi alloys [J]. J Mater Sci, 1987, 22: 123-131.

[2] Predel B, Ratke L and Fredriksson H. Fluid Science and Materials Science in Space: a European Perspective [M]. Walter H U. New York: Springer-Verlag Press, 1987. 517-565.

[3] Walter H U. Materials Science in Space [M]. Feuerbacher B, Hamacher H and Naumann R J. New York: Springer-Verlag Press, 1986. 343-378.

[4] ZHAO Jiu-zhou, GUO Jing-jie and JIA Jun. Ostwald coarsening under changing volume fraction condition [J]. Trans Nonferrous Met Soc China, 1995, 5(1): 67-70.

[5] ZHAO Jiu-zhou, GUO Jing-jie and JIA Jun. Collision coarsening of dispersion droplets in solidification process of monotectic alloy [J]. Trans Nonferrous Met Soc China, 1995, 5(2): 85-87.

[6] ZHAO Jiu-zhou, GUO Jing-jie and JIA Jun. Solidification of Zn-Pb alloy under simulant microgravity condition of orthogonal electric and magnetic fields [J]. Trans Nonferrous Met Soc China, 1995, 5(3): 105-108.

[7] Fredriksson H. Pro RIT/ESA/SSC Workshop on the Effect of Gravity on the Solidification of Immiscible Alloys [R]. ESA, SP-219, Jarva Krog, Sweden, 1984. 25.

[8] Chattopadhyay K and Ramachandrarao P. Rapid solidification and decomposition of a hypomonotectic Al-Cd alloy [J]. J Mater Sci, 1980, 15: 685-692.

[9] Zhang D L and Cantor B. Heterogeneous nucleation of In particles embedded in an Al matrix [J]. Philosophical Magazine A, 1990, 62(5): 557-572.

[10] Goswami R and Chattopadhyay K. Microstructural developments in rapidly solidified monotectic alloys [J]. Mater Sci Eng, 1994, A179/A180: 163-167.

[11] Moore K I and Zhang D L. Solidification of Pb particles embedded in Al [J]. Acta Metall Mater, 1990, 38(7): 1327-1342.

[12] Kim W T, Zhang D L and Cantor B. Microstructure of rapidly solidified aluminium-based immiscible alloy [J]. Mater Sci Eng, 1991, 134A: 1133-1138.

[13] HUANG Z. Microstructure feature in metallic alloy solidified under microgravity [J]. Scripta Metall Mater, 1991, 25: 149-152.

(Edited by PENG Chao-qun)